GEOPHYSICS, VOL. 75, NO. 3 (MAY-JUNE 2010); P. L51–L59, 6 FIGS.
10.1190/1.3378764

Rapid construction of equivalent sources using wavelets

Yaoguo Li[1] and Douglas W. Oldenburg[2]

ABSTRACT

We have developed a fast algorithm for generating an equivalent source by using fast wavelet transforms based on orthonormal, compactly supported wavelets. We apply a 2D wavelet transform to each row and column of the coefficient matrix and subsequently threshold the transformed matrix to generate a sparse representation in the wavelet domain. The algorithm then uses this sparse matrix to construct the the equivalent source directly in the wavelet domain. Performing an inverse wavelet transform then yields the equivalent source in the space domain. Using upward continuation of total-field magnetic data between uneven surfaces as examples, we have compared this approach with the direct solution using the dense matrix in the space domain. We have shown that the wavelet approach can reduce the CPU time by as many as two orders of magnitude.

INTRODUCTION

The equivalent source technique (Dampney, 1969) plays an important role in the processing and interpretation of potential-field data. The technique stems from the special properties of the potential fields. The potential field and its derivatives are harmonic functions in the source-free region. If the field is known on the bounding surface of a region, then the field anywhere in this region is uniquely determined by the solution of a Dirichlet problem in which the boundary condition is given by the known field (Kellog, 1953). Therefore, if one can construct a source distribution outside this region that reproduces the field on the boundary, then it also defines the field in the source-free region. Such source distributions are infinite in number, but only one of them needs to be constructed. Because it usually bears no resemblance to the true source, the term equivalent source is used to describe it. Two important areas of application are the continuation of potential-field data between uneven surfaces (Hansen and Miyazaki, 1984) and the reduction to the pole of magnetic data at low latitudes (Silva, 1986).

Equivalent source construction involves setting up a source layer located below the observation surface and computing its physical property distribution from observed data by solving a linear inversion. Then any linear transformation of potential-field data can be computed from the estimated physical property distribution. Let d be the potential-field data located over an observation surface S_o, and let m be the strength of the equivalent source distributed over a surface S_e. To obtain the best results, the surface S_e coincides with S_o or lies below it, but should be above the actual sources that produced the data d. The integral equation is formally written as

$$d(\mathbf{r}) = \int_{S_e} m(\mathbf{r}')g(\mathbf{r},\mathbf{r}')ds', \quad \mathbf{r} \in S_o \tag{1}$$

where $g(\mathbf{r},\mathbf{r}')$ is the kernel function, whose form depends on the type of the equivalent source; and $\mathbf{r}$ and $\mathbf{r}'$ are the positions of observation and source locations, respectively. Different types of equivalent sources, i.e., the physical properties in the equivalent layer, are used in the literature. Those commonly used include point monopoles, point dipoles, and piecewise constant magnetization distributions.

The construction of the equivalent source requires the inversion of equation 1 to recover an m from the given data d. For numerical solutions, this entails the discretization of the equation. We divide the undulating surface S_e into a set of square cells that are contiguous horizontally and offset vertically, and assume a constant source strength within each cell. This yields a matrix representation

$$\mathbf{d} = \mathbf{Gm}, \tag{2}$$

where $\mathbf{d} = (d_1,\cdots,d_N)^T$ is the vector containing the observed data; $\mathbf{m} = (m_1,\cdots,m_M)^T$ is the vector containing the strength of the equiv-

Manuscript received by the Editor 19 January 2009; revised manuscript received 24 May 2009; published online 21 April 2010.
[1]Colorado School of Mines, Department of Geophysics, Center for Gravity, Electrical, and Magnetic Studies, Golden, Colorado, U.S.A. E-mail: ygli@mines.edu.
[2]University of British Columbia, Department of Earth and Ocean Sciences, UBC Geophysical Inversion Facility, Vancouver, British Columbia, Canada. E-mail: doug@eos.ubc.ca.

alent source; and $\mathbf{G}$ is the coefficient matrix whose elements g_{ij} typically are defined by

$$g_{ij} = \int_{\Delta S_e^j} g(\mathbf{r}_i, \mathbf{r}')ds', \tag{3}$$

where ΔS_e^j is the subarea corresponding to m_j. Here, we assume there are N observations and M equivalent source parameters. The inverse solution of the matrix system in equation 2 yields the numerical solution of the equivalent source.

The coefficient matrix $\mathbf{G}$ is dense. For large data sets, the process is almost prohibitively expensive. For this reason, the equivalent source technique has not gained wide application in potential-field processing. Approximations have been made to reduce the problem to a more manageable size. For instance, Hansen and Miyazaki (1984) use a block-sparse approximation of $\mathbf{G}$ by setting g_{ij} to zero when the distance between the observation and the source is greater than a user-defined range of influence. However, the computational complexity remains in general the biggest hurdle to the effective use of this technique.

To overcome this difficulty, we develop a fast solution method for the equivalent source based on wavelet transforms using orthonormal, compactly supported wavelets. The core of the method is the sparse wavelet representation of the coefficient matrix and a conjugate gradient solution of the resulting system. We achieve further speedup by constructing the equivalent source directly in the wavelet domain. In addition, we use a wavelet-domain model objective function so that the equivalent source solution is stable and consistent with the noise level of the data.

We first develop the sparse wavelet representation of the coefficient matrix. We then formulate the construction as an inverse problem in the wavelet domain. To achieve this, we examine a model objective function that quantifies the spectral properties of the equivalent source using its wavelet coefficients. We next develop the fast numerical solution using the conjugate gradient least-squares (CGLS) strategy. We finally conclude with illustrations using synthetic and field examples.

WAVELET REPRESENTATION OF THE COEFFICIENT MATRIX

In their work on the 3D inversion of magnetic data, Li and Oldenburg (2003) compress the sensitivities of each datum with respect to the unknown susceptibilities by applying a 3D wavelet transform and setting to zero the small wavelet coefficients that are below a given threshold. The resultant sparse representation of the sensitivity matrix composed of the transformed and thresholded sensitivities can achieve compression ratios from 10 to 50. The essence of that operation is the compression of a function because only the variation of sensitivities with the source locations is represented in the wavelet domain and the variation with observation location is left in the space domain. However, in the case of equivalent source construction for regularly spaced data, the wavelet transform can be applied with respect to both the source locations and observation locations. This is consistent with the established method for sparse representation of integral operators in the wavelet bases. As a result, we can achieve a high compression ratio with insignificant errors.

For many applications, gridded data are available. Therefore, we focus on this type of application, as do many previous authors (e.g., Hansen and Miyazaki, 1984; Silva, 1986). This condition is not overly restrictive and enables us to tackle several important problems in potential-field processing. We therefore discretize the equivalent source layer so that there is an m_i corresponding to every d_i; i.e., $N = M$ (we will assume this condition henceforth).

Assume that the observation surface S_o and the equivalent source surface S_e are continuous. Then, the coefficient matrix arising in the construction of an equivalent source layer is characterized by a peak along the diagonal and a smooth decay away from the diagonal. This type of operator is well-suited to being represented sparsely by the wavelet bases as shown by Beylkin et al. (1991) in their seminal paper on fast numerical algorithms using wavelet transforms. For 1D problems, Beylkin et al. (1991) show that when an appropriately chosen wavelet transform is applied to such matrices, the transformed matrix has significant elements only within a narrow band near the location of the peaks in the original matrix. Retaining only these large coefficients and setting the rest to zero produces a sparse representation of the original matrix with a high degree of accuracy. Although that work was proposed within the context of solving the integral equations of the second kind, the methodology for operator compression is applicable to our current problem of inverting the integral equations of the first kind for equivalent source construction.

For completeness, we give a brief review of the wavelet transforms (for details, see, e.g., Daubechies, 1988, 1992). The wavelets are a class of orthonormal bases defined recursively by solving two-scale difference equations (equation 4 below). Let $\psi(x)$ be the wavelet and $\phi(x)$ be its accompanying scaling function; then they are completely defined by

$$\phi(x) = \sqrt{2}\sum_{k=0}^{L-1} h_k \phi(2x-k),$$
$$\psi(x) = \sqrt{2}\sum_{k=0}^{L-1} g_k \phi(2x-k), \tag{4}$$

where h_k and g_k are the wavelet coefficients forming a quadrature mirror filter bank and

$$g_k = (-1)^k h_{L-k}, \quad k = 0,\cdots,L-1. \tag{5}$$

A quadrature mirror filter bank splits a signal into a complementary pair of smooth and detailed components (Strang and Nguyen, 1996). The coefficients are chosen so that the wavelet $\psi(x)$ had n vanishing moments (Daubechies, 1992):

$$\int_{-\infty}^{\infty} \psi(x)x^i dx = 0, \quad i = 1,\cdots, \quad n-1. \tag{6}$$

These wavelets are also well localized in both the space and Fourier domains. The complete set of bases is derived by the translation and dilation of the single function $\psi(x)$:

$$\psi_{j,k}(x) = 2^{-j/2}\psi(2^{-j}x - k), \tag{7}$$

where j denotes the scale and a smaller value corresponds to a coarser scale (i.e., lower resolution).

Using these bases, an orthonormal wavelet transform of a discrete series $\mathbf{v}$ can be formed:

$$\tilde{\mathbf{v}} = \mathbf{W}\mathbf{v}, \tag{8}$$

where $\tilde{\mathbf{v}}$ contains the coefficients of the wavelet transform and $\mathbf{W}$ is the matrix defining the wavelet transform. The explicit form of $\mathbf{W}$ can be found in Press (1992). However, it is almost never used in practice. Instead, the transform is carried out by using the pyramid algorithm (Mallat, 1989), which uses the convolutions of the discrete series with the filter coefficients h_k and g_k. The former extracts the smooth part of the signal and the latter extracts the detailed component. This process is repeated on the subsampled smooth portion until the coarsest representation is obtained. The compression property of the wavelet transform derives from the presence of a large number of small or zero coefficients. These small wavelet coefficients are produced because the wavelets are localized and they are orthogonal to low-order polynomials. The smoothly varying portion of a function can be well represented by only a few wavelets at coarse scales.

The elements in columns of the coefficient matrix $\mathbf{G}$ correspond to different observation locations (x,y) on the surface S_o, and the elements in rows correspond to different source locations (x',y') on S_e. Thus, each row or column can be considered a 2D image. We can apply 1D wavelet transforms along the x- and y-directions, respectively, for each column to obtain a separable 2D wavelet transform. This is exactly analogous to the operation of 2D fast Fourier transform (FFT). The same 2D wavelet transform can be applied to the rows as well. Therefore, applying the 2D wavelet transform to each row and column expands $\mathbf{G}$ in the wavelet bases. Let $\mathbf{W}_2$ be the symbolic matrix representation of the 2D wavelet transform; then the transformed coefficient matrix $\tilde{\mathbf{G}}$ can be written as

$$\tilde{\mathbf{G}} = \mathbf{W}_2\mathbf{G}\mathbf{W}_2^T. \tag{9}$$

Because many elements of $\tilde{\mathbf{G}}$ are nearly or identically zero, they can be discarded when their amplitudes fall below a threshold δ. This leads to the desired sparse matrix $\tilde{\mathbf{G}}_s$ and a discarded matrix $\tilde{\mathbf{G}}' = \tilde{\mathbf{G}} - \tilde{\mathbf{G}}_s$.

Unlike the commonly used soft thresholding in denoising applications, a hard threshold is required for matrix compression because the goal is to discard small coefficients to reduce the storage requirement and the CPU time for matrix-vector multiplications. The threshold δ for winnowing the small coefficients is determined by the required accuracy. Although various matrix norms can be used to define accuracy measures, their effect on the accuracy of forward modeling (i.e., the evaluation of equation 2) often is not apparent. We therefore adopt a more pragmatic approach of using the relative error of the modeled data produced by the thresholding. This is defined as

$$r = \frac{\|\tilde{\mathbf{G}}'\tilde{\mathbf{m}}\|}{\|\tilde{\mathbf{G}}\tilde{\mathbf{m}}\|}, \tag{10}$$

where $\tilde{\mathbf{m}} = \mathbf{W}_2\mathbf{m}$ is the transformed model vector. Because the quantity r is model dependent, we evaluate it using a model $\mathbf{m}$ consisting of uncorrelated random numbers. Numerical tests indicate that the choice of a relative threshold of 0.001, so that $\delta = 0.001 * \max(|\tilde{g}_{ij}|)$, is reasonable for many practical applications. It produces a relative error of about $r \approx 1\%$.

It is important to note that the relative threshold, instead of an absolute threshold, should be specified in practice because the latter is highly dependent on the problem and its scaling. There is a trade-off between computational efficiency and accuracy. A higher relative threshold yields a sparser matrix and faster computation at the cost of accuracy. Thus, one might need to experiment with the relative threshold for specific applications in practice.

As an illustration, we consider the following synthetic problem. The magnetic data are located over a 64×64 grid with an interval of 1 m in both horizontal directions. The data are assumed to be a total-field anomaly with an ambient field in the direction $I = 50°$ and $D = 10°$. We use an equivalent source that is composed of thin rectangular prisms with a constant, vertical magnetization. The prisms are centered beneath each data point. They have a width of 1 m in both horizontal directions and extend beneath the observation surface from 0.1 to 0.6 m. The choice of depth and thickness is not crucial, but it is desirable to have a small depth and a thickness less than the width of the cell so as to better reproduce the high-frequency signal in the data.

The resulting coefficient matrix for this problem is 4096×4096, and it is dense. Applying the wavelet transform using the Daubechies wavelet (Daubechies, 1988) that has three vanishing moments, and thresholding with the above criterion, results in a sparse transformed matrix having only 346,986 nonzero entries. This represents a compression ratio of 48.4. The relative error of the left-hand side is less than 1%. Figure 1 shows the sparsity pattern of the transformed matrix. Each nonzero element is plotted as a black dot, and zero elements are blank. The matrix is dominated by a diagonal band and four off-diagonal bands above and below.

FAST SOLUTION FOR EQUIVALENT SOURCE

We now turn our attention to the construction of an equivalent source using the compressed coefficient matrix. Given that $\mathbf{G}$ is square, one might obtain the solution for $\mathbf{m}$ by the direct inversion of the matrix system, and the observed data are fit exactly. This causes

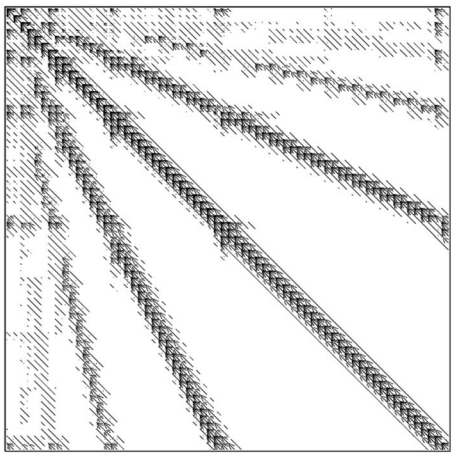

Figure 1. The sparsity pattern of the transformed coefficient matrix after the thresholding has been applied. The matrix has dimensions of 4096×4096. The nonzero elements are shown as black dots, and they represent a 2% fill.

two potential problems. First, the matrix $\mathbf{G}$ might be poorly conditioned, and the direct inversion becomes unstable. Second, the observed data are always contaminated by noise, and the exact inversion of the matrix system is unwise. Therefore, we treat the problem as an inverse problem and solve it by introducing explicit regularization. Thus, our approach differs from the standard equivalent source technique in that we seek to construct an equivalent source layer that only reproduces the signal in the data.

Space-domain formulation

Let ϕ_d be the data misfit quantifying the difference between the observed data and those predicted by the equivalent source, and let ϕ_m be the model objective function quantifying the complexity of the equivalent source. We obtain the inverse solution for the equivalent source by Tikhonov regularization (Tikhonov and Arsenin, 1977):

$$\begin{aligned} &\text{minimize } \phi = \phi_d + \mu\phi_m \\ &\text{subject to } \phi_d = \phi_d^*, \end{aligned} \tag{11}$$

where μ is the regularization parameter and ϕ_d^* is the target misfit, which depends on the estimated error level of the data.

The model objective function imposes desired properties on the constructed equivalent source to achieve stability. For most applications, a model objective that penalizes the size of the equivalent source and its structural complexity is a good choice; hence, we use the form

$$\phi_m = \int\int \left[\alpha_s m^2 + \left(\frac{\partial m}{\partial x}\right)^2 + \left(\frac{\partial m}{\partial y}\right)^2 \right] dxdy. \tag{12}$$

This is a generic model objective function that has been used extensively in applied geophysical inversion (e.g., Dosso and Oldenburg, 1989; Menke, 1989; Li and Oldenburg, 2003). It measures globally the model complexity without being concerned with the position-dependent local properties of the model.

In our current application, we essentially require that the constructed equivalent source is smooth with respect to its lateral location without reference to the vertical position of the source or the corresponding rate of change of observed data as a function of position. Given the assumption that the surface S_e is continuous, such a requirement is reasonable. The smoothness of the model is primarily determined by the parameter $\alpha_s \in [0,\infty)$. Setting $\alpha_s = 0$ yields a maximally smooth equivalent source, and $\alpha_s > 1$ diminishes the effect of the derivative terms in equation 12, which is similar to the damped least-squares approach to equivalent source construction by Leão and Silva (1989). It is important to note that the equivalent source serves only as an intermediate step to achieve the desired data processing such as upward continuation or reduction to the pole; the specific properties of the equivalent source are not important so long as its construction is stable and minimally affected by data noise. Consequently, it often suffices to construct a maximally smooth solution with $\alpha_s = 0$.

The data misfit ϕ_d is defined by

$$\phi_d = \|\mathbf{Gm} - \mathbf{d}\|^2, \tag{13}$$

where $\|\cdot\|$ denotes the L_2 norm. Here, we assume that the data and coefficient matrix have been normalized by the standard deviation of the error in the data. Having defined the data misfit and model objective function, we can proceed with the solution of the minimization problem in equation 11 to construct the equivalent source.

The minimization process involves a search for an optimal μ value that yields the target misfit. In cases when the target misfit is unknown due to the lack of explicit knowledge of data error statistics, μ must be estimated independently by such methods as the L-curve criterion (Hansen, 1998) or generalized cross validation (GCV) (Wahba, 1990). Henceforth, we assume that the target misfit is known and focus on the computational complexity of this basic problem.

The direct approach using the dense matrix would involve discretizing equation 12 using the finite-difference approximation to the derivative operators to obtain

$$\phi_m = \mathbf{m}^T\mathbf{L}^T\mathbf{Lm}, \tag{14}$$

and solving the following system:

$$(\mathbf{G}^T\mathbf{G} + \mu\mathbf{L}^T\mathbf{L})\mathbf{m} = \mathbf{G}^T\mathbf{d}, \tag{15}$$

where $\mathbf{L}^T\mathbf{L}$ is the model weighting matrix representing the model objective function based on the finite-difference approximation. The model weighting matrix is extremely sparse (Menke, 1989) and incurs little computational expense. The impediment to this direct approach comes from the presence of the dense matrix $\mathbf{G}$, which is what we set out to overcome.

The solution of equation 15 can be sped up by performing fast matrix-vector multiplications in the wavelet domain by using the sparse, transformed coefficient matrix $\tilde{\mathbf{G}}_s$. This would be similar to the approach that Li and Oldenburg (2003) take in the fast 3D magnetic inversion. We refer to this as the wavelet-accelerated approach. We have implemented both approaches in the space domain for the purpose of comparison.

Wavelet-domain formulation

Given the availability of $\tilde{\mathbf{G}}_s$, the most efficient route to the solution is to perform the minimization completely in the wavelet domain. We now develop this method. First we apply the wavelet transform to the data $\mathbf{d}$ and represent the model $\mathbf{m}$ in the wavelet bases,

$$\begin{aligned} \tilde{\mathbf{d}} &= \mathbf{W}_2\mathbf{d}, \\ \mathbf{m} &= \mathbf{W}_2^T\tilde{\mathbf{m}}, \end{aligned} \tag{16}$$

where $\mathbf{W}_2$ is the same wavelet transform applied to the coefficient matrix. Then, the original equation 2 can be rewritten as

$$\tilde{\mathbf{d}} = \tilde{\mathbf{G}}\tilde{\mathbf{m}}, \tag{17}$$

and $\tilde{\mathbf{d}}$ and $\tilde{\mathbf{m}}$ become the data and model in the wavelet domain, respectively.

Next, it is necessary to derive the wavelet-domain equivalent of the model objective function in equation 12 and the data misfit in equation 13. For the model objective function, we need to use the Fourier transform as a tool to understand the meaning of equation 12 when the model is represented in the wavelet bases. Express the model in its Fourier transform:

$$m(x,y) = \int_p\int_q f(p,q)e^{i(px+qy)}dpdq, \tag{18}$$

where (p,q) are the transform variables in the x- and y-directions. By Parseval's theorem, the model objective function in equation 12 can be expressed as

$$\phi_m = \int_p \int_q (\alpha_s + p^2 + q^2)|f(p,q)|^2 dpdq. \quad (19)$$

Two interesting points emerge from this transformation. First, the term $(\alpha_s + p^2 + q^2)$ can be viewed as the square of a weighting function applied to the Fourier transform of the model. Thus, a smoothness objective function in the space domain is expressed by a weighted smallest model objective function (i.e., a diagonal weighting function) in the Fourier domain. Second, the weighting function implies a spectral decay of the model that has the form

$$P(p,q) = \frac{1}{\alpha_s + p^2 + q^2} = \frac{1}{\alpha_s + \omega^2}, \quad (20)$$

where $\omega = \sqrt{p^2 + q^2}$ is the radial wavenumber. This represents a statistically self-similar process with a power spectrum obeying an inverse power law. Therefore, by imposing a model objective function of the form in equation 12, we are seeking to construct a self-similar model whose power spectrum decays as $1/\omega^2$.

When a self-similar process is represented in the wavelet bases, the wavelet coefficients on the same scale exhibit uncorrelated Gaussian behavior, the variance decays exponentially with the scale, and the exponent is equal to the product of the scale and the rate of power spectral decay (Flandrin, 1992). In other words, for a process with a power spectrum of the form $1/\omega^\beta$, the variance of the wavelet coefficients at the jth scale is

$$v_j \propto 2^{-j\beta}. \quad (21)$$

This can be extended to multidimensional models when a separable wavelet transform is used:

$$v_{j_x j_y} \propto 2^{-(j_x\beta_x + j_y\beta_y)}, \quad (22)$$

where j_x and j_y are the scales of the wavelet transform in the x- and y-directions, and β_x and β_y are the rates of power spectral decay in the x- and y-directions, respectively. In our current problem, $\beta_x = \beta_y = 2$, and the variance is given by $2^{-2(j_x + j_y)}$.

Given this understanding, a weighting function that is inversely proportional to the standard deviation of the wavelet coefficients at a given scale is required to produce the same type of model as does the space-domain objective function. Thus, the wavelet-domain equivalent of the space-domain objective function in equation 12 is given by

$$\phi_m(\tilde{m}) = \sum_{j_x,j_y} 2^{2(j_x+j_y)} \sum_{k_x,k_y} (\tilde{m}^{k_x,k_y}_{j_x,j_y})^2, \quad (23)$$

where $\tilde{m}^{k_x,k_y}_{j_x,j_y}$ are the wavelet coefficients; and k_x and k_y denote the location index of the wavelet coefficients in the x- and y-directions, respectively. Written in the matrix form,

$$\phi_m(\tilde{\mathbf{m}}) = \tilde{\mathbf{m}}^T \tilde{\mathbf{L}}^T \tilde{\mathbf{L}} \tilde{\mathbf{m}}, \quad (24)$$

where $\tilde{\mathbf{L}}$ is a diagonal matrix given by

$$\tilde{\mathbf{L}} = \mathrm{diag}(\cdots, 2^{(j_x+j_y)}, \cdots), \quad (25)$$

and the entries on the diagonal of $\tilde{\mathbf{L}}$ are ordered in the same way as are the coefficients in $\tilde{\mathbf{m}}$.

We remark that although we have used the Fourier transform to arrive at the new model objective function in equation 23, this step does not rely on the assumption of a planar surface as required in the Fourier-domain processing of potential-field data. Such an assumption is required in potential-field processing so that space-domain operators are expressed as 2D convolutions. Transforming such operations to the Fourier domain leads to decoupled systems that are simple multiplications because of the convolution theorem of the Fourier transform.

However, a 2D Fourier transform can be applied to any 2D function, such as an equivalent source defined on undulating surfaces. Thus, the above result is generally applicable to the equivalent source construction, and the fact that it is on an uneven surface does not pose any difficulties. This is because the model objective function equation 12 is formed as an integral with respect to x and y, and there is no reference to the vertical position of the source. We also note that this result might seem to imply that the wavelet transform $\mathbf{W}_2$ diagonalizes the space-domain weighting matrix $\mathbf{L}^T\mathbf{L}$. This is not strictly true. The direct wavelet transform of $\mathbf{L}^T\mathbf{L}$ is, however, diagonally dominated, and keeping only the diagonal elements would be an excellent approximation. It is for this reason that we use the notation $\tilde{\mathbf{L}}$.

The wavelet-domain misfit function is easily established. Because $\mathbf{W}_2$ is an orthonormal transform and its application to a vector does not change the norm, we have the same form of data misfit in the space and wavelet domains:

$$\phi_d = \|\mathbf{G}\mathbf{m} - \mathbf{d}\|^2 = \|\tilde{\mathbf{G}}\tilde{\mathbf{m}} - \tilde{\mathbf{d}}\|^2. \quad (26)$$

In other words, the misfit function is directly calculable using wavelet-domain quantities.

Substituting equations 24 and 26 into equation 11, and carrying out formal minimization with respect to $\tilde{\mathbf{m}}$, yields

$$(\tilde{\mathbf{G}}^T\tilde{\mathbf{G}} + \mu\tilde{\mathbf{L}}^T\tilde{\mathbf{L}})\tilde{m} = \tilde{\mathbf{G}}^T\tilde{\mathbf{d}}. \quad (27)$$

The matrix $\tilde{\mathbf{G}}$ is replaced by its sparse version $\tilde{\mathbf{G}}_s$ during the computation. This equation has the same appearance as equation 15, but the difference is that all matrices involved in the computation are very sparse. Therefore, equation 27 is much easier to solve even if it is solved by a line search to find the appropriate μ that yields the desired data misfit.

Alternatively, one can use incomplete conjugate gradients (CG) (Haber, 1997) to further reduce the computational cost. The weighting matrix $\tilde{\mathbf{L}}$, as given in equation 25, is diagonal, and it is invertible; thus we can convert equation 27 to a standard form:

$$(\tilde{\mathbf{G}}_L^T\tilde{\mathbf{G}}_L + \mu\mathbf{I})\tilde{\mathbf{m}}_L = \tilde{\mathbf{G}}_L^T\tilde{\mathbf{d}}, \quad (28)$$

where

$$\tilde{\mathbf{G}}_L = \tilde{\mathbf{G}}\tilde{\mathbf{L}}^{-1},$$

$$\tilde{\mathbf{m}}_L = \tilde{\mathbf{L}}\tilde{\mathbf{m}}. \quad (29)$$

This problem can be solved without an explicit regularization parameter μ by incomplete conjugate gradient (CG) least squares

(Haber, 1997). In an incomplete CG solution, we apply only a limited number of CG iterations to

$$\widetilde{\mathbf{G}}_L^T\widetilde{\mathbf{G}}_L\widetilde{\mathbf{m}}_L = \widetilde{\mathbf{G}}_L^T\widetilde{\mathbf{d}}. \tag{30}$$

The number of CG iterations acts as the inverse of the regularization parameter μ in equation 28; i.e., the degree of regularization is inversely proportional to the number of CG iterations performed.

A full CG solution of equation 30 is equivalent to setting $\mu = 0$ in equation 28, whereas a small number of iterations corresponds to a large μ value. In an incomplete CG, we start with $\widetilde{\mathbf{m}} = 0$ and terminate the iteration when the data misfit ϕ_d has been reduced to within an acceptable tolerance from the target value ϕ_d^*, and the resulting model at that iteration provides the solution for the equivalent source construction. The desired equivalent source is obtained by applying $\widetilde{\mathbf{L}}^{-1}$ to $\widetilde{\mathbf{m}}_L$ followed by an inverse wavelet transform. This is by far the most efficient approach.

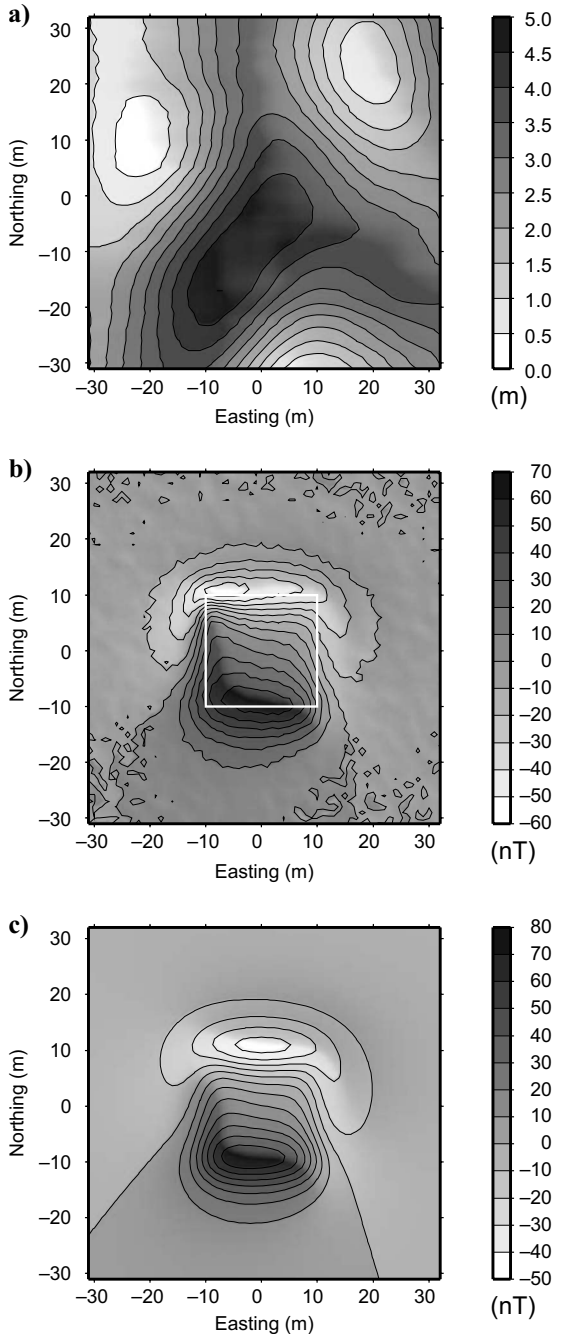

Figure 2. A synthetic example illustrating the equivalent source construction. Maps display (a) the topography, (b) the noise-corrupted total-field anomaly on the uneven surface shown in (a) and produced by a thin vertical prism, and (c) the accurate total-field anomaly on a plane at an elevation of 4 m and produced by the same prism. The prism is outlined by the white lines in (b) and extends vertically from -1 to -3 m in elevation. The magnetization of the prism is 2 A/m and is aligned with the ambient field direction of $I = 50°$ and $D = 10°$.

NUMERICAL EXAMPLES

We illustrate the algorithm using two examples. The first one is a synthetic case designed to demonstrate the validity and efficiency of the wavelet-domain method. As comparisons, we also perform the construction by applying the direct space-domain method using the dense matrix, and the wavelet-accelerated space-domain method using fast matrix-vector multiplications. Figure 2a shows a topographic surface, and Figure 2b and c shows, respectively, the total-field magnetic data on the topographic surface and on a plane intersecting the topography.

Both data sets are produced by the same source body. We simulated the field over a 64×64 grid on each surface. The grid spacing is 1 m in both directions. The causative body is a vertical thin prism with a width of 20 m in both east and north directions and a vertical extent from -1 to -3 m in elevation, and its magnetization is 2 A/m. The magnetization and the ambient field have the same direction of $I = 50°$ and $D = 10°$. The topographic surface has elevations ranging from 0 to 5 m, and the planar surface has an elevation of 4 m. We have added independent Gaussian noise with a standard deviation of 1 nT to the observations on the topographic surface to simulate observed data. The objective is to construct an equivalent source layer for the observed data and continue them to the planar surface.

We use a piecewise constant magnetization distribution as the equivalent source, and choose to align the magnetization direction with the ambient field direction. This choice produces the least amount of distortion near the edges that is sometimes seen in the upward continuation based on the equivalent source. The majority of the planar surface at a 4-m elevation is above the original observation surface, but a portion is below. The equivalent source is placed 0.1 m below the observation surface or the plane, depending on which is lower (Figure 3).

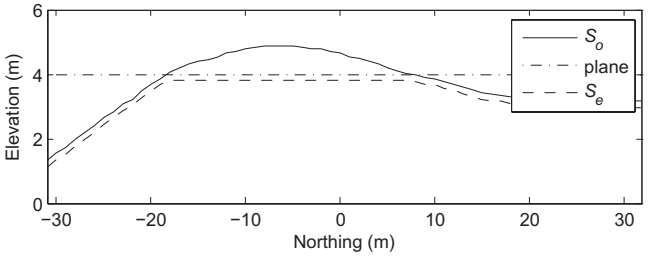

Figure 3. An illustration of relative positions of three surfaces involved in the equivalent source construction. This is a profile corresponding to 0-m east in Figure 2. The solid line indicates the original observation surface (S_o), the dotted-dashed line the plane to which the data are to be continued, and the dashed line the equivalent source surface (S_e).

We have constructed the equivalent source using the direct method (by solving equation 15), wavelet-accelerated method, and wavelet-domain method for comparison. They all produce numerically identical solutions and provide consistent and good representations of the true field at the continuation height. For brevity, we reproduce only the result of the wavelet-domain method here (Figure 4), which took only nine CG iterations to obtain as shown in Figure 5. Figure 4a shows the field continued to the elevation of 4 m using the constructed equivalent source, which compares well with the true field in Figure 2c. The difference between the true field and the continued field (Figure 4a) is shown in Figure 4b. The difference reaches 3 nT at isolated points, but it is mostly within 2 nT. This is a somewhat small deviation considering that the true field has a dynamic range of 130 nT and the observed data are contaminated by noise. However, the important point is that all three approaches have produced the same result that compares well with the true field at the continuation height. This validates the wavelet-domain method.

We now examine the computational efficiency achieved in the wavelet domain by comparing the relative CPU times required to obtain a solution with each method. For the wavelet-accelerated method and wavelet-domain method, we compress the coefficient matrix using the Daubechies wavelet that has three vanishing moments. The resultant sparse matrix in the wavelet domain achieves a compression ratio of 56. The sparsity pattern is similar to that shown in Figure 1. To facilitate the comparison, we denote the CPU time for the wavelet-domain method as 1 unit. The corresponding CPU time for the space-domain and wavelet-accelerated space-domain methods are, respectively, 470 and 4 units. These are the CPU times required to obtain one solution with the correct regularization parameter μ, although practical applications require several such solutions to search for the optimal regularization parameter for the space-domain and wavelet-accelerated methods. The important comparison is between the direct space-domain method and the wavelet-domain method. It is clear that substantial computational savings are achieved through the use of the wavelet transform and incomplete conjugate gradient solution in the wavelet domain.

As a second example, we apply the wavelet-domain method to a set of field data acquired in gold exploration at a low magnetic latitude ($I = -17°$, $D = 1.5°$). Figure 6a displays the surface topography, and Figure 6b is the observed total-field anomaly on the surface. The elevation of the topography varies from 400 to 900 m. The corresponding total-field anomaly varies from −2200 nT to 400 nT. The influence of the rugged topography is apparent in the data. For example, the extremely strong negative anomaly is located at a topography low.

We wish to observe the field on a planar surface at an elevation of 870 m. We use a similar approach as in the synthetic case and place the equivalent source slightly below either the observation surface or the plane, whichever is lower. We achieve a compression ratio of 61, and the incomplete conjugate gradient takes 39 iterations to obtain the desired data misfit. The total-field anomaly continued to the plane (Figure 6c) has much more balanced peak and trough values. The wavelet-domain method has worked well in this field example with strong topographic relief and low magnetic latitude. The computational efficiency is similar also to that seen in synthetic test cases.

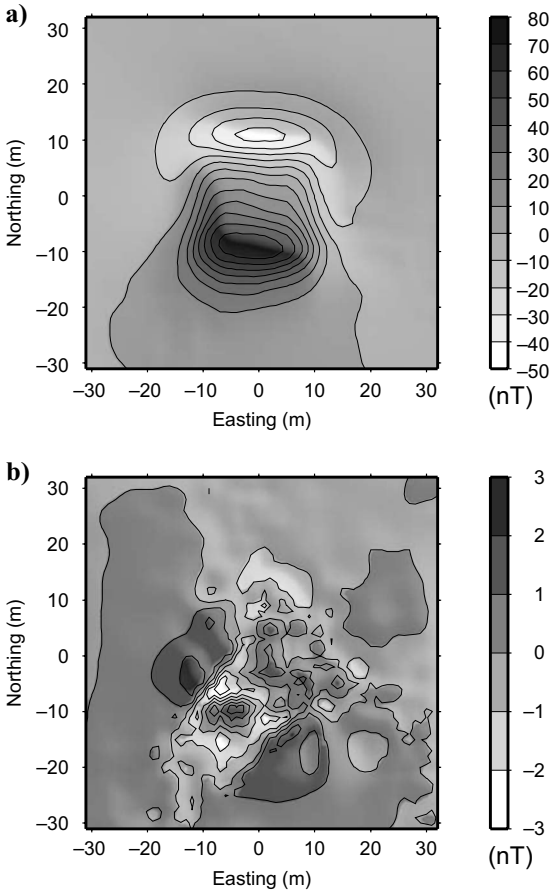

Figure 4. An illustration of the wavelet-domain equivalent source construction for continuation of the magnetic field from an uneven surface to a plane. (a) The continued total-field anomaly at an elevation of 4 m using the equivalent source. This field agrees with the true field shown in Figure 2c. (b) The differences between the two fields. The maximum deviation is 3 nT, but most differences are well below 2 nT.

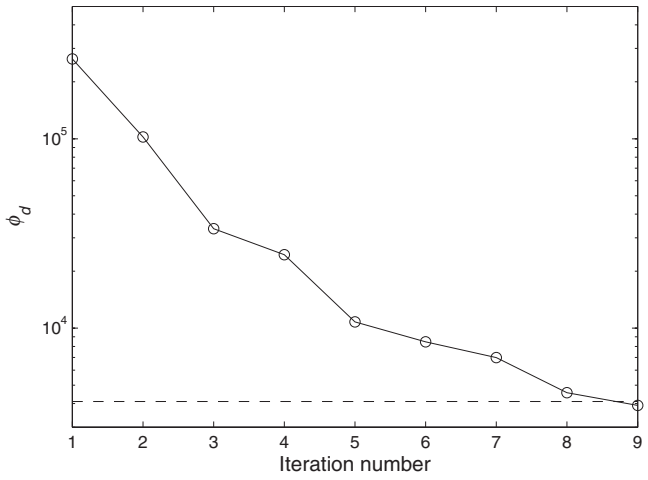

Figure 5. A convergence curve for the wavelet-domain-method construction of an equivalent source in the synthetic example, which uses incomplete conjugate gradient (CG), and the number of iterations serves as the inverse of the regularization parameter. Only nine iterations are required to reach the target misfit indicated by the dashed line.

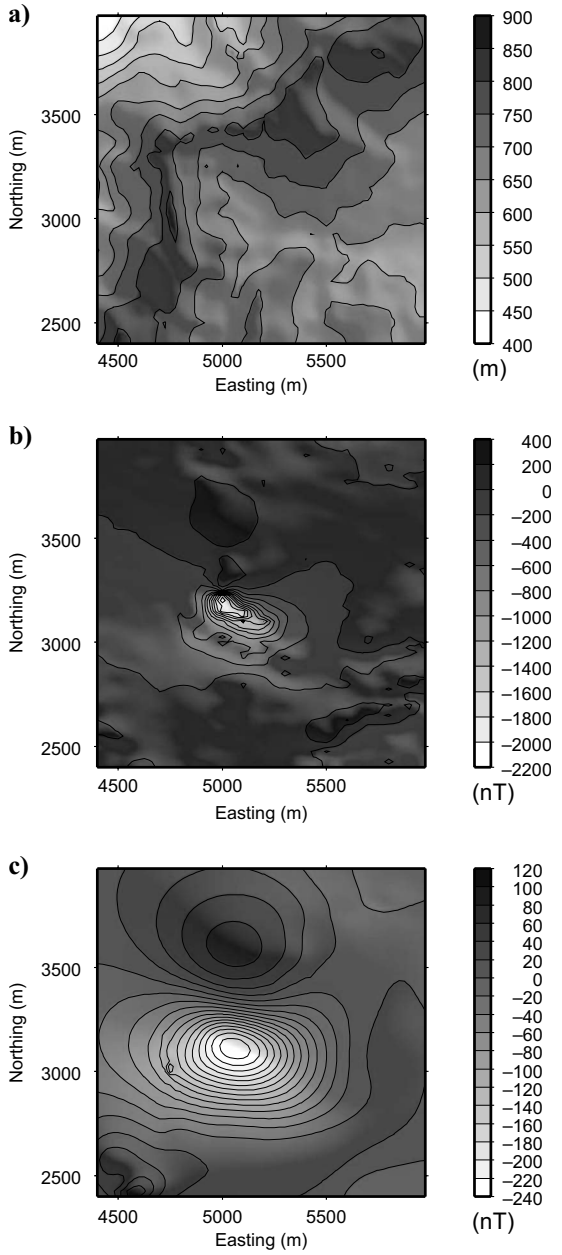

Figure 6. A field example illustrating the continuation between uneven surfaces using the wavelet-domain construction of equivalent sources. (a) The surface topography. (b) The total-field anomaly observed on the topographic surface. The ambient field has an inclination of $-17°$ and a declination of 1.5°. (c) A display of the data continued to a constant elevation of 870 m.

CONCLUSIONS

We have developed a rapid construction algorithm for the equivalent source of potential-field data. The algorithm uses the sparse wavelet representation of operators and a wavelet-domain model objective function. The coefficient matrices involved in the equivalent source problems are well-suited for compression using orthonormal bases of compactly supported wavelets. The compressed matrix can have as low as a few percent of elements to be nonzero. Such a sparse matrix, coupled with a diagonal form of the weighting matrix in the wavelet domain and the use of incomplete conjugate gradient iterations, greatly reduces the computations.

Because the method is based on the compression of the coefficient matrix, the compressibility of the matrix is the deciding factor for its efficiency. The best compression is obtained when the elements of the coefficient matrix peak along the diagonal. Thus, a greater compression ratio is achieved when vertical dipoles, or magnetization, are used for anomalies with steep inclination and when horizontal dipoles are used for anomalies with shallow inclination. Simple dipole sources and magnetized prisms with small vertical extent also produce a better compression ratio. However, the choice of source type must be made to balance the high compression ratio with the quality of the constructed equivalent source. For example, it is observed, independent of the solution method, that the best result for upward continuation is obtained when the direction of the dipole or magnetization is aligned with the direction of the anomaly projection. Other choices of the dipole direction tend to produce larger errors along the edge of the map.

The work reported here serves to prove the concept of the method and demonstrates its efficacy and numerical feasibility. Further efficiency can be achieved by developing direct approaches for calculating the sparse, transformed coefficient matrix or by adopting different wavelets. It is likely that a different wavelet would yield a higher compression ratio, but we have not investigated it exhaustively within the scope of this work. Consequently, this method could fill a gap for processing large data sets collected on undulating surfaces where the Fourier transform-based methods are no longer valid.

ACKNOWLEDGMENTS

We would like to thank Perry Eaton and Newmont Mining Corporation for supplying the field data set used in the study. We also thank the associate editor Valéria C. F. Barbosa, Jeff Phillips, and anonymous reviewers for their detailed comments that helped improve the clarity of the manuscript.

REFERENCES

Beylkin, G., R. Coifman, and V. Rokhlin, 1991, Fast wavelet transforms and numerical algorithms I: Communications on Pure and Applied Mathematics, **44**, 141–183.

Dampney, C. N. G., 1969, The equivalent source technique: Geophysics, **34**, 38–53.

Daubechies, I., 1988, Orthonormal bases of compactly supported wavelets: Communications on Pure and Applied Mathematics, **41**, 909–996.

——, 1992, Ten lectures on wavelets: Society of Industrial and Applied Mathematics.

Dosso, S. E., and D. W. Oldenburg, 1989, Linear and non-linear appraisal using extremal models of bounded variation: Geophysical Journal International, **99**, 483–495.

Flandrin, P., 1992, Wavelet analysis and synthesis of fractal Brownian motion: IEEE Transactions on Information Theory, **38**, 910–917.

Haber, E., 1997, Numerical strategies for the solution of inverse problems: Ph.D. thesis, University of British Columbia.

Hansen, P. C., 1998, Rank-deficient and discrete ill-posed problems: Numerical aspects of linear inversion: Society for Industrial and Applied Mathematics.

Hansen, R. O., and Y. Miyazaki, 1984, Continuation of potential fields between arbitrary surfaces: Geophysics, **49**, 787–795.

Kellog, O. D., 1953, Foundations of potential theory: Dover Publications.

Leão, J. W. D., and J. B. C. Silva, 1989, Discrete linear transformations of potential-field data: Geophysics, **54**, 497–507.

Li, Y., and D. W. Oldenburg, 2003, Fast inversion of large scale magnetic data using wavelet transform and logarithmic barrier method: Geophysical Journal International, **152**, 251–265.

Mallat, S., 1989, A theory for multiresolution signal decomposition: The wavelet representation: IEEE Transactions on Pattern Analysis and Machine Intelligence, **11**, 674–493.

Menke, W., 1989, Geophysical data analysis: Discrete inverse theory: Academic Press.
Press, W. H., S. A. Teukolsky, W. T. Vetterling, and B. P. Flannery, 1992, Numerical recipes in FORTRAN 77: The art of scientific computing: Cambridge University Press.
Silva, J. B. C., 1986, Reduction to the pole as an inverse problem and its application to low-latitude anomalies: Geophysics, **51**, 369–382.
Strang, G., and T. Nguyen, 1996, Wavelets and filter banks: Brooks Cole.
Tikhonov, A., and V. Arsenin, 1977, Solutions of ill-posed problems: Winston and Sons.
Wahba, G., 1990, Spline models for observational data: CBMS-NSF Regional Conference Series in Applied Mathematics, Society for Industrial and Applied Mathematics.